ORNL/TM--8127

DE83 000469

ORNL/TM-8127
Dist. Category UC-20

Contract No. W-7405-eng-26

FUSION ENERGY DIVISION

MASTER

ANALYSIS OF MIXED MODE MICROWAVE DISTRIBUTION MANIFOLDS

T. L. White

DISCLAIMER

This report was prepared as an account of work sponsored by an agency of the United States Government. Neither the United States Government nor any agency thereof, nor any of their employees, makes any warranty, express or implied, or assumes any legal liability or responsibility for the accuracy, completeness, or usefulness of any information, apparatus, product, or process disclosed, or represents that its use would not infringe privately owned rights. Reference herein to any specific commercial product, process, or service by trade name, trademark, manufacturer, or otherwise, does not necessarily constitute or imply its endorsement, recommendation, or favoring by the United States Government or any agency thereof. The views and opinions of authors expressed herein do not necessarily state or reflect those of the United States Government or any agency thereof.

Date Published - September 1982

Prepared by the
OAK RIDGE NATIONAL LABORATORY
Oak Ridge, Tennessee 37830
operated by
UNION CARBIDE CORPORATION
for the
DEPARTMENT OF ENERGY

DISTRIBUTION OF THIS DOCUMENT IS UNLIMITED

Printed in the United States of America. Available from
National Technical Information Service
U.S. Department of Commerce
5285 Port Royal Road, Springfield, Virginia 22161
NTIS price codes—Printed Copy: A03; Microfiche A01

This report was prepared as an account of work sponsored by an agency of the United States Government. Neither the United States Government nor any agency thereof, nor any of their employees, makes any warranty, express or implied, or assumes any legal liability or responsibility for the accuracy, completeness, or usefulness of any information, apparatus, product, or process disclosed, or represents that its use would not infringe privately owned rights. Reference herein to any specific commercial product, process, or service by trade name, trademark, manufacturer, or otherwise, does not necessarily constitute or imply its endorsement, recommendation, or favoring by the United States Government or any agency thereof. The views and opinions of authors expressed herein do not necessarily state or reflect those of the United States Government or any agency thereof.

CONTENTS

ABSTRACT

The 28-GHz microwave distribution manifold used in the ELMO Bumpy Torus-Scale (EBT-S) experiments consists of a toroidal metallic cavity, whose dimensions are much greater than a wavelength, fed by a source of microwave power. Equalization of the mixed mode power distribution to the 24 cavities of EBT-S is accomplished by empirically adjusting the coupling irises which are equally spaced around the manifold. The performance of the manifold to date has been very good, yet no analytical models exist for optimizing manifold transmission efficiency or for scaling this technology to the EBT-P manifold design. The present report develops a general model for mixed mode microwave distribution manifolds based on isotropic plane wave sources of varying amplitudes that are distributed toroidally around the manifold. The calculated manifold transmission efficiency for the most recent EBT-S coupling iris modification is 90%. This agrees with the average measured transmission efficiency. Also, the model predicts the coupling iris areas required to balance the distribution of microwave power while maximizing transmission efficiency, and losses in waveguide feeds connecting the irises to the cavities of EBT are calculated using an approach similar to the calculation of manifold losses. The model will be used to evaluate EBT-P manifold designs.

1. INTRODUCTION

Microwave distribution systems that require high power handling capability and good transmission efficiency relative to the dominant mode waveguide must employ an oversized waveguide. In addition, these requirements can be realized only if spurious propagating modes are controlled by careful design of system components to minimize spurious mode conversion and if mode-selective absorbers are used to damp out spurious mode resonances.[1] This paper analyzes a new distribution system approach using a mixed mode microwave distribution manifold that has very good power handling capability and high transmission efficiency and yet does not require mode control. In fact, a large number of modes are intentionally excited to improve the distribution of power from the mixed mode manifold.

The technique for distributing microwave power is to feed an oversized, low loss, metallic cavity with a source of microwave power. Distribution of the microwaves is accomplished by opening a number of holes or "irises" in the cavity wall. The dimensions of the cavity are much, much greater than a free space wavelength, and the cavity can contain a large number of possible modes. A large number of modes are excited by making the cavity shape irregular and by randomly scattering the incoming microwave power so that the incoming mode is severely distorted upon reflection from the scattering surface. The discrete but complex mode pattern within the cavity is continually perturbed, which gives a completely smooth frequency response. Examples of these kinds of systems are acoustic reverberation chambers,[2] microwave untuned cavities,[3] and the microwave distribution manifold used in electron cyclotron heating experiments on EBT-S[4] (see Fig. 1).

For simplicity, we shall first consider a weak coupling model and then generalize the weak coupling model to include strong coupling with a balanced distribution of microwave power. The strong coupling model is compared to data obtained on the EBT-S 28-GHz microwave distribution manifold for two different iris distributions. Also, the losses in the connecting feeds between the manifold and the microwave loads are calculated. The results can be used to scale the EBT-S manifold to other geometries and frequencies.

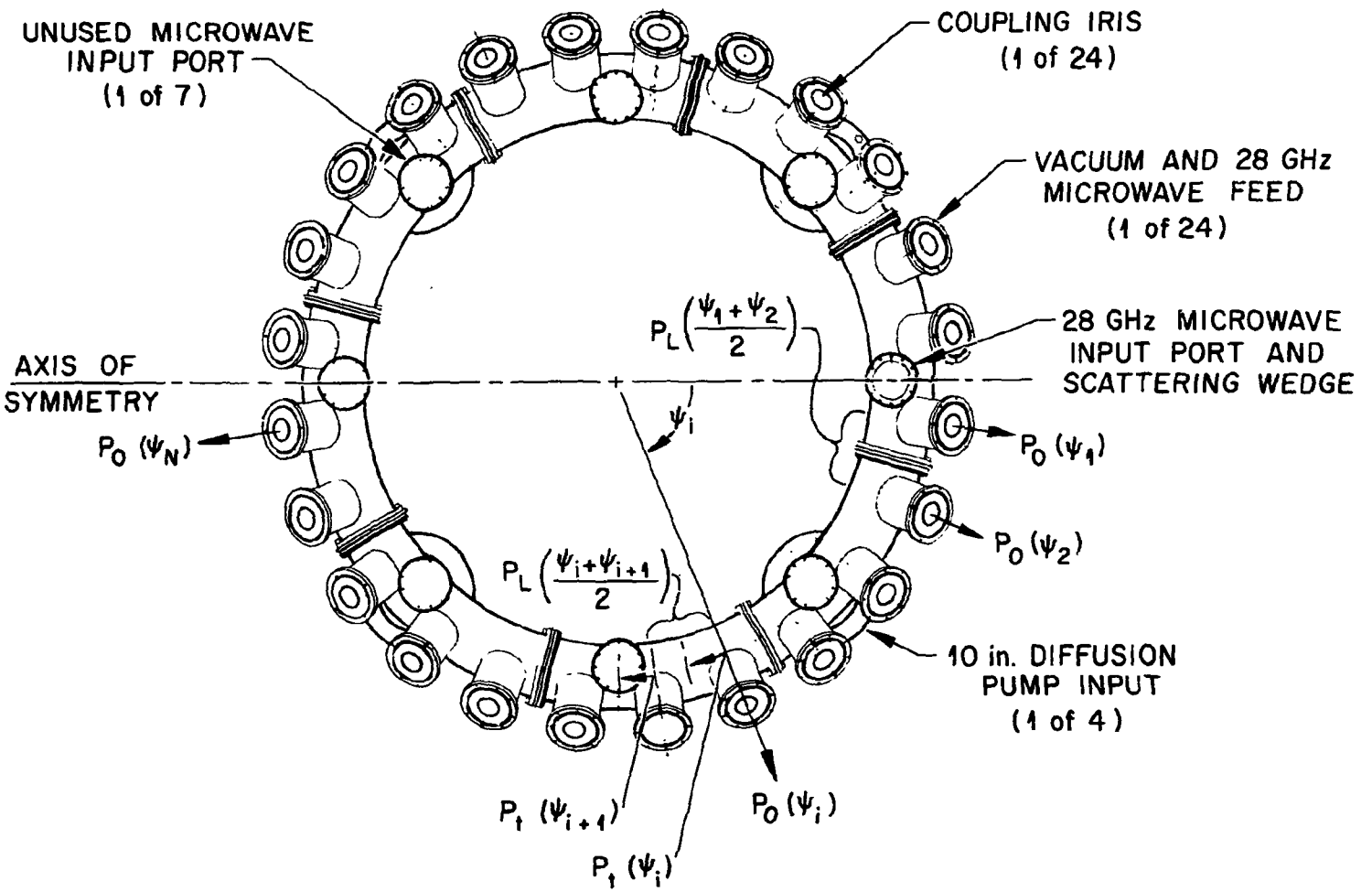

Fig. 1. EBT-S 28-GHz microwave distribution system.

2. WEAK COUPLING THEORY

The complex nature of the electromagnetic fields in such an irregular cavity does not lend itself to analysis on a mode by mode basis; however, the "randomness" of the mode distribution can be exploited in computing average quantities that describe the electrical behavior of the cavity. We approach the problem by expressing the microwave fields in the cavity as a sum of a large number of plane waves propagating in free space at all angles within the cavity. This can be done because any cavity mode can be expressed by a superposition of a number of plane waves. We begin by calculating the power in a single plane wave after a wall reflection as a function of angle of incidence θ for both polarizations given by

$$P_r = \frac{1}{2} \mathrm{Re} \int_A [(\vec{E}_{\perp r} \times \vec{H}^*_{\parallel r}) + (\vec{E}_{\parallel r} \times \vec{H}^*_{\perp r})] \cdot \vec{n} \, dA \, , \tag{1}$$

where

P_r = average power reflected,
dA = incremental surface area,
$\vec{n}$ = surface normal,
$\vec{E}$ = cavity electric field,

and

$\vec{H}$ = cavity magnetic field.

The r subscript refers to reflected quantities and the $\perp$ and $\parallel$ subscripts imply fields that are perpendicular and parallel, respectively, to the plane of incidence (defined as the plane containing $\vec{n}$ and $\vec{k}$, as shown in Fig. 2). Here, we assume that the surface is flat on a scale greater than a wavelength where $\vec{k}$ is the unit vector in the direction of propagation and the i subscript refers to incident quantities. The large number of mixed or scrambled modes in a cavity with small losses guarantees a uniform distribution of power over the surface of the cavity, and we can rewrite Eq. (1) as

ORNL-DWG 81-19332 FED

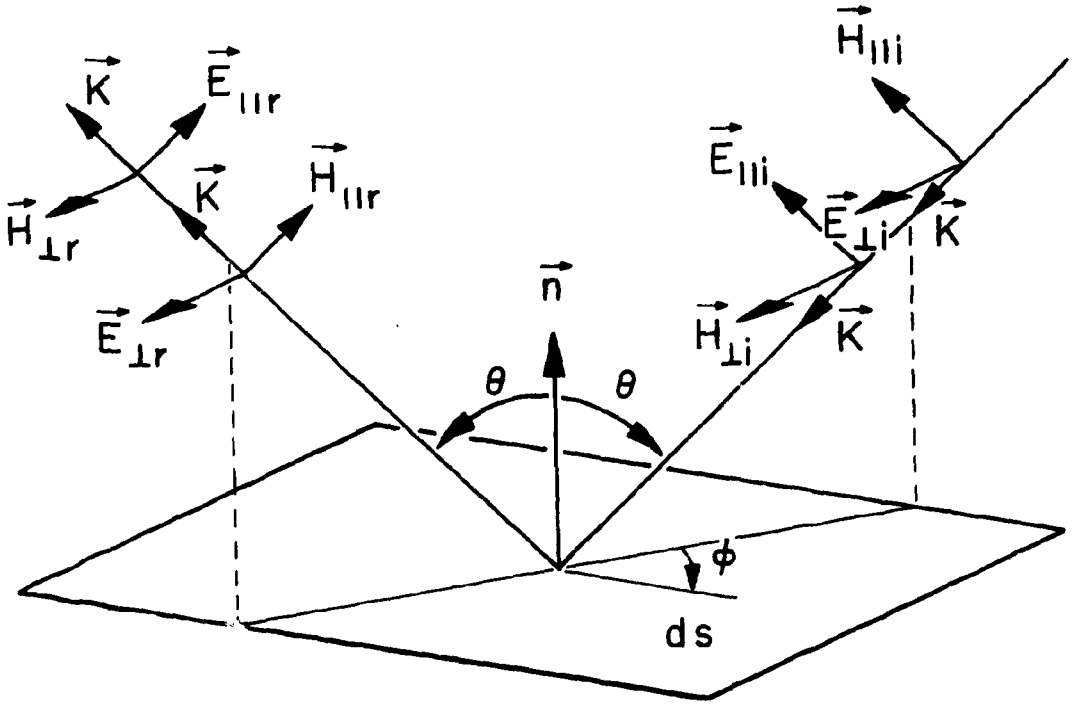

Fig. 2. Plane wave reflection on a plane metallic boundary.

$$P_r = \frac{A_c \cos\theta}{2\eta} \left(|\vec{E}_{\perp r}|^2 + |\vec{E}_{\parallel r}|^2\right) , \tag{2}$$

where

A_c = cavity surface area,

η = impedance of free space = $\sqrt{\frac{\mu_0}{\varepsilon_0}}$,

$\cos\theta = \vec{n} \cdot \vec{k}$,

μ_0 = permeability of free space,

and

ε_0 = permittivity of free space.

We have made use of the fact that for a plane wave

$$\vec{H}_{\perp} = \frac{-\vec{E}_{\parallel}}{\eta} , \tag{3}$$

and

$$\vec{H}_{\parallel} = \frac{\vec{E}_{\perp}}{\eta} . \tag{4}$$

By the same method we can calculate the plane wave power incident prior to the reflection as

$$P_i = \frac{A_c \cos\theta}{2\eta} \left(|\vec{E}_{\perp i}|^2 + |\vec{E}_{\parallel i}|^2\right) . \tag{5}$$

The power lost in the reflection is

$$P_L = P_i - P_r \tag{6}$$

or

$$P_L = \frac{A_c \cos\theta}{2\eta} \left[|\vec{E}_{\perp i}|^2 (1 - r_\perp^2) + |\vec{E}_{\parallel i}|^2 (1 - r_\parallel^2) \right] , \tag{7}$$

where $r_\perp^2$ and $r_\parallel^2$ are the power reflection coefficients given by Stratton[5] for a plane wave incident on a plane surface of a good electrical conductor:

$$r_\perp^2 \equiv \frac{|\vec{E}_{\perp r}|^2}{|\vec{E}_{\perp i}|^2} \approx 1 - 2 \sqrt{\frac{2\varepsilon_0 \omega}{\sigma}} \cos\theta \tag{8}$$

and

$$r_\parallel^2 \equiv \frac{|\vec{E}_{\parallel r}|^2}{|\vec{E}_{\parallel i}|^2} \approx 1 - 2 \frac{\sqrt{2\varepsilon_0 \omega/\sigma}}{\cos\theta} , \tag{9}$$

assuming

$$\sqrt{\frac{2\varepsilon_0 \omega}{\sigma}} << 1,$$

with

σ = electrical conductivity,

and

$\omega = 2\pi f$ = radian frequency.

For a random mix of a large number of modes, we assume that the power in both polarizations is approximately equal so that

$$|\vec{E}_{\perp i}|^2 = |\vec{E}_{\parallel i}|^2 = |\vec{E}|^2 ; \tag{10}$$

thus,

$$P_L = \frac{A_c \sqrt{2\varepsilon_0 \omega/\sigma}\ |\vec{E}|^2}{\eta} (1 + \cos^2\theta) \ . \tag{11}$$

Now, we can average over half a spherical surface at the wall of the cavity,

$$P_{LAV} = \frac{1}{2\pi} \int_0^{2\pi} \int_0^{\pi/2} P_L \sin\theta \, d\theta \, d\phi \tag{12}$$

or

$$P_{LAV} = \frac{8R_s A_c |\vec{E}|^2}{3\eta^2} \ , \tag{13}$$

where P_{LAV} is the average power lost to the walls and

$$R_s = \sqrt{\frac{\pi f \mu_0}{\sigma}} \tag{14}$$

is the surface resistivity of the metal.

We can define the cavity Q (or quality factor) as

$$Q \equiv \frac{\omega U}{P_{LAV}} \tag{15}$$

where

U = total energy stored in the cavity for both polarizations,

and

$\omega = 2\pi f$ = radian frequency.

The stored energy can be written as

$$U = \varepsilon(|\vec{E}_{\perp i}|^2 + |\vec{E}_{\parallel i}|^2)V_c \ , \tag{16}$$

where V_c = cavity volume. Then, assuming equal power in both polarizations,

$$U = 2\varepsilon|\vec{E}|^2 V_c \ , \tag{17}$$

and after some manipulations,

$$Q = \frac{3V_c}{2A_c\delta} \ , \tag{18}$$

where

$$\delta = \text{electrical skin depth} = \frac{1}{\sqrt{\pi f \mu_0 \sigma}} \ . \tag{19}$$

This result agrees with the results of Lamb,[6] who uses a somewhat different photon model to calculate Q.

The next step is to calculate the transmission efficiency for a cavity with weak coupling to microwave loads, subject to the constraint that the dimensions of each coupling iris be much greater than a free space wavelength. This allows us to neglect diffraction effects in connection with the coupling irises. Furthermore, the total iris area is much less than the cavity area in order to ensure weak coupling. If the iris area is made too large, we will spoil the uniform energy density in the cavity. However, we shall consider this case later when we treat strong coupling.

The power coupled out of the ith iris is written as

$$P_{iOUT} = \frac{1}{2}\,\mathrm{Re}\int_{iris} [(\vec{E}_{\perp i} \times \vec{H}^*_{\parallel i}) + (\vec{E}_{\parallel i} \times \vec{H}^*_{\perp i})] \cdot dA_i \,\vec{n} \ , \tag{20}$$

where dA_i = ith iris incremental area and $\vec{E}$ and $\vec{H}$ are the cavity electric and magnetic fields, respectively. However,

$$(\vec{E}_{\perp} \times \vec{H}^*_{\parallel}) \cdot \vec{n} = \cos\theta \frac{|\vec{E}_{\perp i}|^2}{\eta} , \tag{21}$$

$$(\vec{E}_{\parallel i} \times \vec{H}^*_{\perp i}) \cdot \vec{n} = \cos\theta \frac{|\vec{E}_{\parallel i}|^2}{\eta} , \tag{22}$$

and, as before,

$$|\vec{E}_{\perp i}|^2 = |\vec{E}_{\parallel i}|^2 = |\vec{E}|^2 . \tag{23}$$

Thus,

$$P_{iOUT} = \frac{\cos\theta \, A_i |\vec{E}|^2}{\eta} . \tag{24}$$

Now, we average over all angles, and

$$\overline{P}_{iOUT} = \frac{1}{2\pi} \int_0^{2\pi} \int_0^{\pi/2} P_{iOUT} \sin\theta \, d\sigma \, d\phi \tag{25}$$

or

$$\overline{P}_{iOUT} = \frac{A_i |\vec{E}|^2}{2\eta} . \tag{26}$$

The total power coupled out is

$$P_{OUT} = \sum_{i=1}^{K} \overline{P}_{iOUT} \tag{27}$$

or

$$P_{OUT} = \frac{A_T |\vec{E}|^2}{2\eta} , \tag{28}$$

where

$$A_T = \sum_{i=1}^{K} A_i = \text{total iris area},$$

A_i = ith iris area,

and

K = total number of irises .

The power balance is written as

$$P_{IN} = P_{LAV} + P_{OUT} \tag{29}$$

and

$$T \equiv \frac{P_{OUT}}{P_{IN}} = \frac{1}{1 + P_{LAV}/P_{OUT}} , \tag{30}$$

where T is the transmission efficiency. Substituting Eqs. (13) and (28) into Eq. (30) we have

$$T = \left(1 + \frac{16 R_s A_c}{3\eta A_T}\right)^{-1} \tag{31}$$

with $\lambda^2 << A_T << A_c$ and $\lambda^2 << A_i$.

3. STRONG COUPLING THEORY

If a mixed mode cavity is used as a distribution manifold, then it is highly desirable to increase the transmission efficiency by increasing the iris areas. Under these circumstances the energy density in the cavity will no longer be uniform but will begin to vary spatially around the cavity. Also, in order to maintain a balance of power distribution, the iris areas must change accordingly to restore the equality of power coupled out of the various irises. In EBT-S an oversized toroidal manifold is used to distribute power 24 ways (neglecting unfed cavities) from a single input. The injected microwave energy is scattered roughly equally in both directions around the torus by employing a scattering wedge. To simplify the analysis we assume that the manifold has an axis of symmetry about the feed point. The manifold is shown schematically in Fig. 1. The energy density in the manifold is proportional to $|\vec{E}(\psi)|^2$, where ψ is the toroidal angle. The measured manifold losses are about 10% of the input power to the manifold, and the loss per section (which is just 1/24th of the total losses) is 1/24 × 10% or 0.417%. This is much less than the power coupled out per manifold section (1/24 × 90%). We can therefore assume that the energy density in the individual manifold section is approximately constant and that the energy density drops in a stepwise fashion at each iris going away from the input feed. We can write the expression for the total manifold losses by summing the individual contributions in each section as

$$P_L = P_L(\psi_1) + 2 \sum_{i=2}^{N} P_L\left(\frac{\psi_{i-1} + \psi_i}{2}\right) + P_L(\psi_N) \ , \qquad (32)$$

where N is equal to half the number of irises. Using Eq. (13) we can express the power loss in each section in terms of an equivalent electric field or

$$P_L = \frac{8R_s A_c}{3\eta^2 K}\left[\left|\vec{E}(\psi_1)\right|^2 + \left|\vec{E}(\psi_N)\right|^2\right] + 2\sum_{i=2}^{N}\frac{8R_s A_c}{3\eta^2 K}\left|\vec{E}\left(\frac{\psi_{i-1}+\psi_1}{2}\right)\right|^2 , \tag{33}$$

where we have assumed that the manifold area per section is constant and

$$\left|\vec{E}\left(\frac{\psi_{i-1}+\psi_i}{2}\right)\right|^2 \approx \frac{\left|\vec{E}(\psi_{i-1})\right|^2 + \left|\vec{E}(\psi_i)\right|^2}{2} . \tag{34}$$

Thus,

$$P_L = \frac{8R_s A_c}{3\eta^2 K}\sum_{i=1}^{K}\left|\vec{E}(\psi_i)\right|^2 . \tag{35}$$

The power coupled out of the irises is given by

$$P_{OUT} = \sum_{i=1}^{K}\frac{A_i\left|\vec{E}(\psi_i)\right|^2}{2\eta} = TP_{IN} , \tag{36}$$

and for a complete balance in power coupled out, we demand that

$$\frac{TP_{IN}}{K} = \frac{A_i\left|\vec{E}(\psi_i)\right|^2}{2\eta} . \tag{37}$$

Now, using Eqs. (30), (35), (36), and (37) we can solve for the transmission efficiency given by

$$T = \left(1 + \frac{16R_s A_c}{3\eta A_{eff}}\right)^{-1} , \tag{38}$$

where

$$A_{eff} = K^2\left(\sum_{i=1}^{K}\frac{1}{A_i}\right)^{-1} . \tag{39}$$

We can recover Eq. (31) from Eq. (38) if $A_{eff} = A_T$, implying that all iris areas are the same. Therefore, our model for strong coupling reduces to our first model for weak coupling if we fix all iris areas the same. Having all irises equal in area, given a balanced power distribution, is equivalent to a uniform energy density in the manifold, and this implies weak coupling.

To solve for the iris areas we must write a recursion relation between the power transmitted into the i<u>th</u> manifold section and the power transmitted into the (i + 1)<u>th</u> section as

$$P_t(\psi_{i+1}) = P_t(\psi_i) - P_{OUT}(\psi_i) - P_L\left(\frac{\psi_i + \psi_{i+1}}{2}\right) \tag{40}$$

or

$$\frac{A_x|\vec{E}(\psi_{i+1})|^2}{2\eta} = \frac{A_x|\vec{E}(\psi_i)|^2}{2\eta} - \frac{A_i|\vec{E}(\psi_i)|^2}{2\eta} - \frac{8R_sA_{ci}}{3\eta^2}\left[\frac{|\vec{E}(\psi_i)|^2 + |\vec{E}(\psi_{i+1})|^2}{2}\right], \tag{41}$$

where A_x is the manifold cross-sectional area and A_{ci} is the area of the i<u>th</u> manifold section. Solving for the ratio of the electric fields squared, we define

$$F_i \equiv \left|\frac{\vec{E}(\psi_{i+1})}{\vec{E}(\psi_i)}\right|^2 = \frac{A_x - (8R_sA_{ci}/3\eta) - A_i}{A_x + (8R_sA_{ci}/3\eta)}. \tag{42}$$

However, power balance requires that

$$\frac{A_i|\vec{E}(\psi_i)|^2}{2\eta} = \frac{A_{i+1}|\vec{E}(\psi_{i+1})|^2}{2\eta} \tag{43}$$

or

$$\left| \frac{E(\psi_{i+1})}{E(\psi_i)} \right|^2 = \frac{A_i}{A_{i+1}} . \tag{44}$$

Substituting Eq. (44) into Eq. ( ) and solving for A_i, we get

$$A_i = \frac{(A_x - 8R_s A_{ci}/3\eta)A_{i+1}}{A_x + 8R_s A_{ci}/3\eta + A_{i+1}} . \tag{45}$$

For an optimum taper, A_N is chosen to be as large as possible because the Nth iris is farthest away from the input. The remainder of the iris areas are determined by the above expression.

4. COMPARISON WITH EXPERIMENT

To analyze an arbitrary distribution of iris areas for the EBT-S manifold, we must go back to Eq. (35), but now we assume that the ith manifold section area varies around the manifold or

$$P_L = \frac{8R_s}{3\eta^2} \sum_{i=1}^{K} A_{ci} |\vec{E}(\psi_i)|^2 . \tag{46}$$

Using Eq. (42) we can write

$$\sum_{i=1}^{K} A_{ci} |\vec{E}(\psi_i)|^2 = |\vec{E}(\psi_1)|^2 \left(A_{c1} + \sum_{i=2}^{K} A_{ci} \prod_{j=1}^{i-1} F_j \right), \tag{47}$$

and

$$\sum_{i=1}^{K} A_i |\vec{E}(\psi_i)|^2 = |\vec{E}(\psi_1)|^2 \left(A_1 + \sum_{i=2}^{K} A_i \prod_{j=1}^{i-1} F_j \right) . \tag{48}$$

Substituting Eqs. (47) and (48) into Eqs. (46) and (36), respectively, and substituting the resulting two equations into Eq. (30), we have

$$T = \left[1 + \frac{16R_s \left(A_{ci} + \sum_{i=2}^{K} A_{ci} \prod_{j=1}^{i-1} F_j \right)}{3\eta \left(A_i + \sum_{i=2}^{K} A_i \prod_{j=1}^{i-1} F_j \right)} \right]^{-1} . \quad (49)$$

Table 1 summarizes the data from two different iris modifications used on the EBT-S microwave distribution manifold.

The data from Table 1 were used in Eq. (49) to calculate the manifold transmission efficiency for both iris modifications, and the results are compared to measured values using standard flow calorimetry techniques on the distribution manifold cooling. The results of the comparison are shown on Table 2.

The errors in the calculated values for T are due to uncertainties in calculating A_{ci} for the various manifold sections, and the errors in the measured values, T_{meas}, represent one standard deviation in the data. Considering the number of simplifying assumptions that have gone into Eq. (49), the results are quite good. Another test of the model would be to produce a distribution of iris areas according to Eq. (45) for optimum power balance and then to measure the resulting distribution of microwave power. Unfortunately, on EBT-S microwave power is not measured directly, and instead perpendicular stored energy of the hot electron rings formed by the microwave power input is measured as a substitute means of power measurement.

5. CALCULATION OF FEED LOSSES

Once power has been distributed by a mixed mode manifold, it must be coupled to the loads by suitable lengths of oversized waveguide. The losses in the guide are a function of the mix of modes available for coupling, which in this case is a random mix of a large number of waveguide modes. If there is a sufficiently large number of modes available for coupling, we expect that a plane wave representation will suffice. Using an approach identical to the calculation of manifold wall losses, we can write an expression for the losses in the walls of the waveguide feeds using Eq. (11), which is repeated here as

Table 1. EBT-S microwave distribution manifold data

EBT-S iris designation	Iris No.	A_i for modification No. 5 (cm^2)	A_i for modification No. 6 (cm^2)	A_{ci} (cm^2)
W1	1	10.10	12.27	1524
W2	2	11.20	13.81	2792
W3	3	12.38	15.52	2792
W4	4	13.61	17.32	4462
W5	5	14.94	19.31	2792
W6	6	16.40	21.38	2792
N1	7	17.72	23.60	3359
N2	8	19.33	25.97	2792
N3	9	0	0	2792
N4	10	22.28	31.14	4462
N5	11	23.93	33.96	2792
N6	12	25.65	36.94	2792

$A_x = 324\ cm^2$

$R_s = 3.17 \times 10^{-7} \sqrt{f}$ ohms

$\eta = 376.734$ ohms

$f = 2.786 \times 10^{10}$ Hz

Table 2. Comparison of theory and experiment

	T [see Eq. (49)] (%)	T_{meas} (%)
Iris Mod. No. 5	87.1 ± 1	89.1 ± 0.95
Iris Mod. No. 6	89.9 ± 1	89.9 ± 0.47

$$P_L = \frac{A_f \sqrt{2\varepsilon_0\omega/\sigma}\ |\vec{E}|^2}{\eta} (1 + \cos^2\theta) \ , \tag{50}$$

where

$A_f = \pi D z$,

D = waveguide feed diameter,

z = waveguide feed length,

and

$\lambda << D$.

If the loads are perfectly absorbing (nonreflecting), we have only a one-way power flow, which is equivalent to averaging over θ from 0 to $\pi/2$ and averaging over ϕ from 0 to π. Therefore,

$$P_{LAV} = \frac{1}{2\pi} \int_0^{\pi} \int_0^{\pi/2} P_L \sin\theta \, d\theta \, d\phi \tag{51}$$

or

$$P_{LAV} = \frac{4R_s A_f |\vec{E}|^2}{3\eta^2} \ . \tag{52}$$

Next, we calculate the total power transferred, which is given by Eq. (26) and rewritten here as

$$P_T = \frac{(\pi D^2/4)|\vec{E}|^2}{2\eta} \ , \tag{53}$$

where the waveguide cross-sectional area is used as the iris area and α, the amplitude attenuation factor per unit length, is

$$\alpha \equiv \frac{P_{LAV}}{2P_T} \ . \tag{54}$$

The transmission efficiency T_f for the waveguide feed is

$$T_f = \exp(-2\alpha z) = \exp\left(-\frac{32R_s z}{3\eta D}\right), \tag{55}$$

where we have made use of Eqs. (52), (53), and (54). The total transmission efficiency from the input of the manifold to a load is simply the product of the above expression and Eq. (38), giving the total transmission efficiency T_t as

$$T_t = \frac{\exp(-32R_s z/3\eta D)}{1 + (16R_s A_c/3\eta A_{eff})}, \tag{56}$$

where

R_s = surface resistivity = $\sqrt{\frac{\pi f_0}{\sigma}}$,

η = impedance of free space,

z = waveguide feed length,

D = waveguide feed diameter,

A_c = manifold surface area,

and

$$A_{eff} = K^2\left(\sum_{i=1}^{K}\frac{1}{A_i}\right)^{-1} = \text{effective iris area.}$$

The above expression will be used to calculate manifold and feed transmission efficiencies for the EBT-P device, and the results will be written up in a later report.

ACKNOWLEDGMENT

The author wishes to thank H. O. Eason for many fruitful discussions and for providing the author with data on the EBT-S 28-GHz microwave distribution manifold.

REFERENCES

1. J. P. Quine, *Microwave Power Engineering*, Vol. I (E. C. Okress, ed.), pp. 178-213, Academic Press, New York, 1968.
2. V. O. Knudsen, J. Acous. Soc. Am. 5, 112-21 (1933).
3. D. T. Llewellyn-Jones, R. J. Knight, P. H. Moffat, and H. A. Gebbie, Proc. IEEE Part A 127, 535-40 (1980).
4. H. O. Eason, G. F. Pierce, T. L. White, and R. E. Wintenberg, paper presented at *1979 IEEE Int. Conf. on Plasma Science*, Montreal, June 4-6, 1979.
5. J. A. Stratton, *Electromagnetic Theory*, pp. 507-508, McGraw-Hill, New York, 1941.
6. W. E. Lamb, Phys. Rev. 70, 308-17 (1946).

ORNL/TM-8127
Dist. Category UC-20

INTERNAL DISTRIBUTION

1. R. N. Adams
2. F. W. Baity
3. L. A. Berry
4. E. S. Bettis
5. A. L. Boch
6. J. S. Brodkowicz
7. N. B. Bryson
8. J. A. Cobble
9. R. J. Colchin
10. R. A. Dory
11. H. O. Eason
12. A. C. England
13. J. C. Glowienka
14. G. A. Hallock
15. D. L. Hillis
16. S. Hiroe
17. H. D. Kimrey
18. E. F. Jaeger
19. O. V. Jett
20. C. M. Loring
21. H. C. McCurdy
22. T. J. McManamy
23. D. H. Metzler
24. O. B. Morgan
25. D. A. Rasmussen
26. R. K. Richards
27. L. Solensten
28. D. A. Spong
29. J. D. Stout
30. D. W. Swain
31. J. S. Tolliver
32. N. A. Uckan
33. T. Uckan
34-38. T. L. White
39. J. B. Wilgen
40-41. Laboratory Records Department
42. Laboratory Records, ORNL-RC
43. Fusion Energy Division Reports Office
44-45. Fusion Energy Division Library
46-47. Central Research Library
48. Document Reference Section
49. ORNL Patent Office

EXTERNAL DISTRIBUTION

50. W. B. Ard, McDonnell Douglas Astronautics Company, Building 107, P.O. Box 516, St. Louis, MO 63166
51. H. L. Berk, Fusion Theory Institute, University of Texas, P.O. Box 7728, Austin, TX 78712
52. Bibliothek, Institut fur Plasmaphysik, D-8046 Garching bei Munchen, Federal Republic of Germany
53. Bibliothek, Institut fur Plasmaphysik, KFA, Postfach 1913, D-5170, Julich 1, Federal Republic of Germany
54. Bibliotheque, Service du Confinement des Plasmas, CEA, B.P. No. 6, 92 Fontenay-aux-Roses (Seine), France
55. N. Bowen, Princeton Plasma Physics Laboratory, P.O. Box 451, Princeton, NJ 08540
56. J. D. Callen, Department of Nuclear Engineering, University of Wisconsin, Madison, WI 53706
57. R. W. Conn, School of Engineering and Applied Science, 6291 Boelter Hall, University of California, Los Angeles, CA 90024
58. R. A. Dandl, Applied Microwave Concepts, 2210 Encinitas Boulevard, Encinitas, CA 92024
59. S. O. Dean, Director, Fusion Energy Development, Science Applications, Inc., 2 Professional Drive, Suite 249, Gaithersburg, MD 20760

60. R. J. DeBellis, McDonnell Douglas Astronautics Company, Building 107, P.O. Box 516, St. Louis, MO 63166
61. J. Doane, Princeton Plasma Physics Laboratory, P.O. Box 451, Princeton, NJ 08540
62. Documentation S.I.G.N., B.P. 85 Centre de Tri, 38041 Cedex, Grenoble, France
63. W. R. Ellis, Advanced Fusion Systems Branch, Office of Fusion Energy, Office of Energy Research, Mail Station G-256, Department of Energy, Washington, DC 20545
64. S. J. Evans, Varian Associates, 611 Hansen Way, Palo Alto, CA 94303
65. A. J. Favle, Grumman Aerospace Corporation, South Oyster Bay Road, P.O. Box 31, Bethpage, NY 11714
66. H. K. Forsen, Bechtel Group, Inc., Research Engineering, P.O. Box 3965, San Francisco, CA 94105
67. M. Fujiwara, Institute of Plasma Physics, Nagoya University, Nagoya 464, Japan
68. T. V. George, Office of Fusion Energy, Office of Energy Research, Mail Station G-256, Department of Energy, Washington, DC 20545
69. G. G. Gibson, Westinghouse Electric Corporation, Fusion Power Systems, Department C, P.O. Box 10864, Pittsburgh, PA 15236
70. R. W. Gould, Department of Applied Physics, California Institute of Technology, Pasadena, CA 92024
71. F. Hockett, McDonnell Douglas Astronautics Company, Building 107, Level 2, Mail Stop 142, P.O. Box 516, St. Louis, MO 63166
72. H. Hsuan, Princeton Plasma Physics Laboratory, P.O. Box 451, Princeton, NJ 08540
73. H. Ikegami, Institute of Plasma Physics, Nagoya University, Nagoya 464, Japan
74. Institute of Physics, Academia Sinica, Peking, Peoples Republic of China
75. H. R. Jory, Varian Associates, 611 Hansen Way, Palo Alto, CA 94303
76. N. A. Krall, Jaycor, 11011 Torreyana Road, P.O. Box 85154, San Diego, CA 92138
77. K. Krause, Lawrence Livermore National Laboratory, P.O. Box 808, Livermore, CA 94550
78. J. Lassoon, TRW Defense and Space Systems, 1 Space Park, Redondo Beach, CA 92078
79. N. H. Lazar, TRW Defense and Space Systems, 1 Space Park, Redondo Beach, CA 92078
80. Library, Centre de Recherches en Physique des Plasmas, 21 Avenue des Bains, 1007 Lausanne, Switzerland
81. Library, Culham Laboratory, UKAEA, Abingdon, Oxon, OX14-3DB, England
82. Library, FOM Institute voor Plasma-Fysica, Rijnhuizen, Jutphaas, Netherlands
83. Library, Institute for Plasma Physics, Nagoya University, Nagoya 464, Japan
84. Library, International Centre for Theoretical Physics, Trieste, Italy
85. Library, Laboratoria Gas Ionizzati, Frascati, Italy
86. Library, Plasma Physics Laboratory, Kyoto University, Gokasho Uji, Kyoto, Japan
87. D. G. McAlees, Exxon Nuclear Company, Inc., 777 106th Avenue, NE, Bellevue, WA 98009

88. J. B. McBride, Science Applications, Inc., 1200 Prospect Street, P.O. Box 2351, La Jolla, CA 92037
89. C. Moeller, General Atomic Company, 10955 John Jay Hopkins Drive, San Diego, CA 92121
90. J. Mullen, McDonnell Douglas Astronautics Company, Building 107, P.O. Box 516, St. Louis, MO 63166
91. Plasma Research Laboratory, Australian National University, P.O. Box 4, Canberra ACT, 2000, Australia
92. P. J. Reardon, Princeton Plasma Physics Laboratory, P.O. Box 451, Princeton, NJ 08540
93. F. L. Ribe, 319 Benson Hall, BF 10, Department of Nuclear Engineering, University of Washington, Seattle, WA 98195
94. W. M. Stacey, School of Nuclear Engineering, Georgia Institute of Technology, Atlanta, GA 30332
95. B. W. Stallard, Lawrence Livermore National Laboratory, P.O. Box 808, Livermore, CA 94550
96. Thermonuclear Library, Japan Atomic Energy Research Institute, Naka, Ibaraki, Japan
97. J. M. Turner, Office of Fusion Energy, Office of Energy Research, Mail Station G-256, Department of Energy, Washington, DC 20545
98. R. Varma, Physical Research Laboratory, Navangpura, Ahmedabad, India
99. H. Weitzner, New York University, Courant Institute of Mathematical Sciences, 251 Mercer Street, New York, NY 10012
100. Office of the Assistant Manager for Energy Research and Development, Oak Ridge Operations Office, Department of Energy, Oak Ridge, TN 37830

101-207. Given distribution as shown in TID-4500, Magnetic Fusion Energy (Distribution Category UC-20)